# Transport Coefficients of Helical Wormlike Chains. 4. Intrinsic Viscosity of the Touched-Bead Model

**Takenao Yoshizaki, Itaru Nitta, and Hiromi Yamakawa***

*Department of Polymer Chemistry, Kyoto University, Kyoto 606, Japan.*
*Received May 27, 1987; Revised Manuscript Received July 16, 1987*

ABSTRACT: The intrinsic viscosity of the helical wormlike touched-bead model without excluded volume is evaluated by taking into account the effect of the finite volume of the bead. An empirical interpolation formula for it is presented. This formula is useful for an analysis of experimental data for flexible chains, if the data for low molecular weights are included. Some salient aspects of the behavior of the intrinsic viscosity over a wide range of molecular weight (or contour length) are discussed on the basis of the numerical results. In particular, it is found that the slope of the double-logarithmic plot of the intrinsic viscosity against the molecular weight becomes smaller than $^1/_2$ as the helical nature becomes strong. Finally, an analysis of experimental data is made for atactic poly(methyl methacrylate) and poly(dimethylsiloxane), and it is concluded that both of these chains may be represented by the helical wormlike chain rather than by the wormlike chain.

## Introduction

In previous papers,[1-3] parts 1–3 of this series, we evaluated the translational friction (or diffusion) coefficient and the intrinsic viscosity of the helical wormlike (HW) chain[4,5] (without excluded volume) by an application of the Oseen–Burgers (OB) procedure of hydrodynamics to the cylinder model. In those papers, we also presented the interpolation formulas both for the translational friction coefficient and for the intrinsic viscosity and showed some examples of stiff chains whose configurational and transport behavior may be explained by the HW chain but not by the ordinary Kratky–Porod (KP) wormlike chain.[6,7] For all of these examples, the static stiffness parameter $\lambda^{-1}$ was rather large ($\lambda^{-1} \gtrsim 100$ Å).

In the case of flexible chains having smaller $\lambda^{-1}$ ($\lesssim$100 Å), we know many of those that cannot be mimicked by the KP chain over a wide range of contour length $L$, and it is necessary to make an analysis of experimental data for their transport coefficients on the basis of the HW chain, if the data for low molecular weights are included. However, for flexible chains, the ratio of the cylinder diameter $d$ to $\lambda^{-1}$ is rather large ($\lambda d \sim 1$), and then the numerical OB solution cannot be obtained for small $\lambda L$ because of the nature of the OB kernel. Thus the above interpolation formula for the intrinsic viscosity, which has been constructed for $\lambda d \lesssim 0.08$, is not valid for flexible chains. Therefore we must adopt another hydrodynamic model to obtain necessary theoretical values. Note that such a problem does not occur as far as the translational friction coefficient is concerned.

Thus, in this paper, we use the touched-bead model as the alternative to evaluate the intrinsic viscosity of the HW chain (without excluded volume). As mentioned above, for flexible chains, we must derive an expression for it that is valid over a wide range of molecular weight including the oligomer region. As the chain becomes shorter, the effect of the finite volume of the bead on the hydrodynamic properties cannot be neglected. Therefore, we take it into account by distributing the frictional force on the surface of the bead instead of regarding the bead as a point force. In anticipation of results, we note that the intrinsic viscosity of this model can then be written as a sum of the solution of the Kirkwood–Riseman equation and the contribution of the Einstein sphere. We solve numerically the Kirkwood–Riseman equation (a set of linear simultaneous equations for the frictional forces) without converting it into an integral equation as was done by them.[8]

In section II, we formulate the intrinsic viscosity of the HW touched-bead model having the finite volume. In section III, we construct an interpolation formula for the intrinsic viscosity on the basis of the numerical solutions and show some salient aspects of its behavior. In section IV, we make an analysis of experimental data for the intrinsic viscosity for atactic poly(methyl methacrylate) and poly(dimethylsiloxane).

## Formulation

Consider a chain composed of $N$ identical spherical beads of diameter $d_b$ whose centers are located on the HW chain contour of total length $L$. The contour distance between two adjacent centers is set equal to the bead diameter $d_b$, i.e., $Nd_b = L$. Thus, the model is defined by the four model parameters: the constant curvature $\kappa_0$ and torsion $\tau_0$ of the characteristic helix[4] of the HW chain, the (static) stiffness parameter $\lambda^{-1}$, and $d_b$, assuming that Poisson's ratio $\sigma$ is zero, as usual. Strictly speaking, two adjacent beads do not touch but slightly overlap, since the contour distance between their centers is longer than the straight distance. The difference between these two distances is negligibly small, so that we call this model the HW touched-bead model. In what follows, all lengths are measured in units of $\lambda^{-1}$ unless specified otherwise.

Now, suppose that the chain is immersed in a solvent having an unperturbed steady shear flow field $\mathbf{v}^0$ at $\mathbf{R}$,

$$\mathbf{v}^0(\mathbf{R}) = \epsilon_0 \mathbf{e}_x\mathbf{e}_y\cdot\mathbf{R} \tag{1}$$

where the molecular center of mass is fixed at the origin of a Cartesian coordinate system ($\mathbf{e}_x$,$\mathbf{e}_y$,$\mathbf{e}_z$), and $\epsilon_0$ is the velocity gradient. Let $\mathbf{S}_p$ be the vector position of the center of the $p$th bead ($p$ = 1, 2, ..., $N$) and $\mathbf{r}_p$ be the radius vector of a point on the surface of the $p$th bead from its center, i.e., $|\mathbf{r}_p| = d_b/2$. Then the chain rotates around the $z$ axis with the angular velocity $\omega = -(1/2)\epsilon_0\mathbf{e}_z$, and the velocity $\mathbf{U}_p(\mathbf{r}_p)$ of that point relative to the unperturbed flow at $\mathbf{r}_p$ is given by

$$\mathbf{U}_p(\mathbf{r}_p) = -\epsilon_0\mathbf{m}\cdot(\mathbf{S}_p + \mathbf{r}_p) \tag{2}$$

with

$$\mathbf{m} = \tfrac{1}{2}(\mathbf{e}_x\mathbf{e}_y + \mathbf{e}_y\mathbf{e}_x) \tag{3}$$

Let $\mathbf{f}_p(\mathbf{r}_p)$ be the frictional force exerted on the fluid by the unit area at $\mathbf{r}_p$ of the surface of the $p$th bead. The intrinsic viscosity $[\eta]$ may then be written in terms of $\mathbf{f}_p$ as follows:[9]

$$[\eta] = -\frac{N_A}{M\eta_0\epsilon_0}\mathbf{m}:\Big\langle \sum_{p=1}^{N}\int_{S_p}\mathbf{f}_p(\mathbf{r}_p)(\mathbf{S}_p + \mathbf{r}_p)\,d\mathbf{r}_p\Big\rangle$$
$$= -\frac{N_A}{M\eta_0\epsilon_0}\sum_{p=1}^{N}\Big[\mathbf{m}:\langle\mathbf{F}_p\mathbf{S}_p\rangle + \mathbf{m}:\Big\langle\int_{S_p}\mathbf{f}_p(\mathbf{r}_p)\mathbf{r}_p\,d\mathbf{r}_p\Big\rangle\Big] \tag{4}$$

0024-9297/88/2221-0165$01.50/0 

where $N_A$ is the Avogadro number, $\eta_0$ is the viscosity coefficient of the solvent, $M$ is the polymer molecular weight, $\langle\ \rangle$ denotes an equilibrium configurational average, $\int_{S_p} d\mathbf{r}_p$ indicates the integration over the surface of the $p$th bead, and $\mathbf{F}_p$ is the total frictional force exerted by the $p$th bead,

$$\mathbf{F}_p = \int_{S_p} \mathbf{f}_p(\mathbf{r}_p)\, d\mathbf{r}_p \tag{5}$$

Under the nonslip boundary condition, the frictional force distribution $\mathbf{f}_p$ satisfies the coupled integral equation,

$$\mathbf{U}_p(\mathbf{r}_p) = (8\pi\eta_0)^{-1} \int_{S_p} \mathbf{k}_p(\mathbf{r}_p,\mathbf{r}'_p)\cdot\mathbf{f}_p(\mathbf{r}'_p)\, d\mathbf{r}'_p + \sum_{\substack{q=1 \\ \neq p}}^{N} \int_{S_q} \mathbf{T}(\mathbf{R}_{pq} - \mathbf{r}_p + \mathbf{r}_q)\cdot\mathbf{f}_q(\mathbf{r}_q)\, d\mathbf{r}_q \tag{6}$$

where $\mathbf{R}_{pq} = \mathbf{S}_q - \mathbf{S}_p$, $\mathbf{T}$ is the Oseen tensor,

$$\mathbf{T}(\mathbf{R}) = (8\pi\eta_0 R)^{-1}(\mathbf{I} + \mathbf{RR}/R^2) \tag{7}$$

with $\mathbf{I}$ the unit tensor, and $\mathbf{K}$ is the tensor defined by

$$\mathbf{K}_p(\mathbf{r}_p,\mathbf{r}'_p) = 8\pi\eta_0\mathbf{T}(\mathbf{r}'_p - \mathbf{r}_p) \tag{8}$$

Now, we make further developments to derive an expression for $[\eta]$ convenient for numerical computation by the use of eq 4 and 6 with eq 2 along the same line as in ref 9. For this purpose, it is convenient to rewrite eq 6 as follows. We expand $\mathbf{T}(\mathbf{R}_{pq} - \mathbf{r}_p + \mathbf{r}_q)$ in eq 6 in a Taylor series around $\mathbf{R}_{pq}$, and neglect terms of $\mathcal{O}(R_{pq}^{-n})$ $(n \geq 2)$. Note that it is equivalent to replacing $\mathbf{T}(\mathbf{R}_{pq} - \mathbf{r}_p + \mathbf{r}_q)$ by $\mathbf{T}(\mathbf{R}_{pq})$. Then, we obtain

$$\mathbf{f}_p(\mathbf{r}_p) = -8\pi\eta_0\epsilon_0 \int_{S_p} \mathbf{K}_p^{-1}(\mathbf{r}_p,\mathbf{r}'_p)\mathbf{r}'_p\, d\mathbf{r}'_p : \mathbf{m} - 8\pi\eta_0 \int_{S_p} \mathbf{K}_p^{-1}(\mathbf{r}_p,\mathbf{r}'_p)\, d\mathbf{r}'_p \cdot [\epsilon_0\mathbf{m}\cdot\mathbf{S}_p + \sum_{\substack{q=1 \\ \neq p}}^{N} \mathbf{T}(\mathbf{R}_{pq})\cdot\mathbf{F}_q] \tag{9}$$

where the tensor $\mathbf{K}_p^{-1}(\mathbf{r}_p,\mathbf{r}'_p)$ is defined by

$$\delta^{(2)}(\mathbf{r}_p - \mathbf{r}'_p)\mathbf{I} = \int_{S_p} \mathbf{K}_p^{-1}(\mathbf{r}_p,\mathbf{r}''_p)\cdot\mathbf{K}_p(\mathbf{r}''_p,\mathbf{r}'_p)\, d\mathbf{r}''_p = \int_{S_p} \mathbf{K}_p(\mathbf{r}_p,\mathbf{r}''_p)\cdot\mathbf{K}_p^{-1}(\mathbf{r}''_p,\mathbf{r}'_p)\, d\mathbf{r}''_p \tag{10}$$

with $\delta^{(2)}(\mathbf{R})$ the two-dimensional Dirac delta function.

First, the tensor $\langle\mathbf{F}_p\mathbf{S}_p\rangle$ is the square brackets in the second line of eq 4 may be obtained as the solutions of a set of simultaneous linear equations. It is derived by multiplying eq 9 by $\mathbf{S}_r$ from the right, integrating over $\mathbf{r}_p$, and averaging over the chain configuration with the equilibrium distribution function, as follows,

$$\langle\mathbf{F}_p\mathbf{S}_q\rangle = -3\pi\eta_0 d_b\epsilon_0\mathbf{m}\cdot\langle\mathbf{S}_p\mathbf{S}_q\rangle - \tfrac{1}{2}d_b \sum_{\substack{r=1 \\ \neq p}}^{N} \langle R_{pr}^{-1}\rangle\langle\mathbf{F}_r\mathbf{S}_q\rangle \tag{11}$$

where we have preaveraged the Oseen tensor and used the following relations:[9]

$$8\pi\eta_0 \int_{S_p} d\mathbf{r}_p \int_{S_p} d\mathbf{r}'_p\, \mathbf{K}_p^{-1}(\mathbf{r}_p,\mathbf{r}'_p) = 3\pi\eta_0 d_b\mathbf{I} \tag{12}$$

$$8\pi\eta_0 \int_{S_p} d\mathbf{r}_p \int_{S_p} d\mathbf{r}'_p\, \mathbf{K}_p^{-1}(\mathbf{r}_p,\mathbf{r}'_p)\mathbf{r}'_p = 0 \tag{13}$$

Equation 12 is the Stokes formula for the friction coefficient of a rigid sphere, and eq 13 indicates that the rigid sphere has a vanishing shear force triadic.[10]

Next we evaluate the second term in the square brackets in the second line of eq 4. Multiplying eq 9 by $\mathbf{r}_p$ from the right, integrating over $\mathbf{r}_p$, and making a double-dot product of the result and the symmetric tensor $\mathbf{m}$, we obtain[9]

$$\mathbf{m}:\int_{S_p} \mathbf{f}_p(\mathbf{r}_p)\mathbf{r}_p\, d\mathbf{r}_p = -\tfrac{5}{12}\pi d_b^3\eta_0\epsilon_0 \tag{14}$$

where we have again used eq 13. Note that the right-hand side of eq 14 is independent of the chain configuration and is equal to the intrinsic viscosity of the Einstein sphere multiplied by $-M\eta_0\epsilon_0/N_A$.

Finally, the intrinsic viscosity $[\eta]$ may be written from eq 4, 11, and 14, as the sum of the solution $[\eta]_{KR}$ of the Kirkwood–Riseman equation and the contribution $[\eta]_E$ of the Einstein spheres,

$$[\eta] = [\eta]_{KR} + [\eta]_E \tag{15}$$

where

$$[\eta]_{KR} = -\frac{N_A}{M}\sum_{p=1}^{N} \phi_{pp} \tag{16}$$

$$[\eta]_E = 5\pi N_A N d_b^3/12M \tag{17}$$

In eq 16, $\phi_{pq}$ is defined by

$$\phi_{pq} = \frac{1}{\eta_0\epsilon_0}\mathbf{m}:\langle\mathbf{F}_p\mathbf{S}_q\rangle \tag{18}$$

and is the solution of the simultaneous linear equations

$$\phi_{pq} + \tfrac{1}{2}d_b \sum_{\substack{r=1 \\ \neq p}}^{N} \langle R_{pr}^{-1}\rangle\phi_{rq} = -\tfrac{1}{2}\pi d_b\langle\mathbf{S}_p\cdot\mathbf{S}_q\rangle \tag{19}$$

In eq 19, $\langle R_{pq}^{-1}\rangle$ is given by

$$\langle R_{pq}^{-1}\rangle = \langle R^{-1}(|p - q|d_b)\rangle \tag{20}$$

where $\langle R^{-1}(s)\rangle$ is the mean reciprocal end-to-end distance of the HW chain of contour length $s$ and is given by eq A1 of ref 11, and the moment $\langle\mathbf{S}_p\cdot\mathbf{S}_q\rangle$ is given by

$$\langle\mathbf{S}_p\cdot\mathbf{S}_q\rangle = (Nd_b/\pi)g[(2p - 1)/N - 1,(2q - 1)/N - 1] \tag{21}$$

where $g(x,y)$ is given by eq 16 of ref 3.

## Empirical Equations and Numerical Results

In this section, we construct empirical interpolation formulas for the Kirkwood–Riseman contributions $[\eta]_{KR}$ to the intrinsic viscosities of the KP and HW chains on the basis of the values calculated from eq 16 with 19. All numerical work has been done by the use of FACOM M-780 and VP-200 digital computers in this university.

Before proceeding further, we make some remarks on the numerical solutions of eq 19. As is well-known, the solutions of the Kirkwood–Riseman equations such as eq 19 possess singularities when the ratio $\xi$ of the diameter of the bead to the spacing is nearly equal to or greater than unity.[12] And it leads to the negative translational diffusion coefficients[12] and the negative intrinsic viscosity.[13] In the case of a rigid rod with the preaveraged Oseen tensor, these singularities never appear in the range of $\xi \leq 1$, including the case of the touched-bead model. (Note that these singularities appear in this range if we use the nonaveraged Oseen tensor.) However, these singularities appear in the case of the HW touched-bead model as the helical nature becomes strong and the diameter $d_b$ becomes large, since the contour of the HW chain locally takes a helical form and the spacing of the beads becomes shorter than in the case of the rigid rod. Thus, we omit the numerical solution if its value seems obviously ridiculous.

Now, we construct an empirical interpolation formula for the factor $\Gamma_{KP}$ defined by

$$[\eta]_{KR}^{(KP)} = (6^{3/2}\Phi_\infty\langle S^2\rangle_{KP}^{3/2}/M)\Gamma_{KP}(L,d_b) \tag{22}$$

Table I
Values of $\alpha_{ij}$ and $\beta_{ij}$ in Equation 26

| $i$ | $\alpha_{i0}$ | $\alpha_{i1}$ | $\alpha_{i2}$ | $\beta_{i0}$ | $\beta_{i1}$ |
|---|---|---|---|---|---|
| 0 | −9.6291 | 1.6198 (2) | 1.1316 (2) | −1.5358 | 9.4913 (2) |
| 1 | −2.3491 | −1.4420 (2) | −2.0502 (3) | −2.3605 | −3.4732 (3) |
| 2 | 5.4811 (1)[a] | −4.8402 (2) | 4.1942 (3) | 1.0550 (1) | 4.0771 (3) |
| 3 | −6.2255 (1) | 7.8877 (2) | −2.6846 (3) | −1.1528 (1) | −1.1290 (3) |
| 4 | 3.0814 (−1) | −4.5617 | 1.5182 | −1.9421 | −3.1301 |
| 5 | −5.1619 | 1.6758 (1) | −4.0308 | 5.1951 (−1) | 1.2811 (1) |
| 6 | 2.9298 | −1.3380 (1) | −2.6757 | 1.1938 (−1) | −9.9978 |
| 7 | −6.2856 (−1) | 1.6070 | 7.4332 | −8.2021 (−2) | −2.8832 |

[a] $a(n)$ means $a \times 10^n$.

where $[\eta]_{KR}^{(KP)}$ is the Kirkwood–Riseman contribution to the intrinsic viscosity of the KP touched-bead model, $\Phi_\infty = 2.870 \times 10^{23}$, and $\langle S^2\rangle_{KP}$ is the mean-square radius of gyration of the KP chain of total contour length $L = Nd_b$ and is given by

$$\langle S^2\rangle_{KP} = \frac{L}{6} - \frac{1}{4} + \frac{1}{4L} - \frac{1}{8L^2}(1 - e^{-2L}) \quad (23)$$

(Note that eq 23 has been derived originally by Benoit and Doty.[15]) The factor $\Gamma_{KP}$ thus defined approaches unity as $L$ becomes infinitely large, i.e.,

$$\lim_{L\to\infty} \Gamma_{KP} = 1 \quad (24)$$

We evaluate $\Gamma_{KP}$ by the use of the values $[\eta]_{KR}$ calculated from eq 16 with the numerical solutions of eq 19 for various values of $d_b$ ranging from 0.01 to 0.8. The number of beads $N$ is limited to 2–1000 because of the capacity of our digital computers. Thus, for small $d_b$, the contour length $L$ is limited to small values, and then the difference between $[\eta]_{KR}^{(KP)}$ and the intrinsic viscosity in the Gaussian limit (given by eq 22 with $\Gamma_{KP} = 1$) is not small. In the case of the rigid rod, it was shown that $[\eta]$ of the touched-bead model with the bead diameter $d_b$ may well be reproduced by $[\eta]$ of the cylinder model having the cylinder diameter $d = 0.724d_b$.[16] Therefore, it is reasonable to adopt the values of $[\eta]$ of the KP cylinder model having the cylinder diameter properly chosen as those of the KP touched-bead model in the range of large $L$ where the numerical solution for the latter cannot be obtained. It has been found that the values of $[\eta]_{KR}^{(KP)}$ obtained numerically are smoothly joined to those of $[\eta]$ of the KP cylinder model calculated from eq 23 and 25 with eq 24 and 26–31 of ref 3 at $N(=L/d_b) \simeq 1000$ in the range of $0.01 \le d_b \le 0.8$ if we take $d = 0.74d_b$. Figure 1 shows the values of $\Gamma_{KP}^{-1}$ thus joined, taking the cases of $d_b = 0.1$ and 0.8 as examples, where the open circles represent the values of the KP touched-bead model, and the full curves represent those of the KP cylinder model with $d = 0.74d_b$.

A good approximation to $\Gamma_{KP}^{-1}$ thus obtained numerically has been found to be of the form

$$\Gamma_{KP}^{-1} = 1 + e^{-5L}\sum_{i=0}^{3} C_i L^{i/2} + e^{-1/4L}\sum_{i=4}^{7} C_i L^{-(i-3)/2} \quad (25)$$

with

$$C_i = \sum_{j=0}^{2} \alpha_{ij} d_b^{\,j} + \sum_{j=0}^{1} \beta_{ij} d_b^{\,2j} \ln d_b \quad (26)$$

where $\alpha_{ij}$ and $\beta_{ij}$ are constants independent of $L$ and $d_b$ and are given in Table I. We note that eq 22 with eq 23, 25, and 26 is applicable for $0.01 \le d_b \le 0.8$, and for the integral values of $L/d_b$ when $2 \le L/d_b \le 1000$ and for all values of $L/d_b$ when $L/d_b \ge 1000$, and the error in the value of $[\eta]_{KR}^{(KP)}$ calculated from them does not exceed 1%.

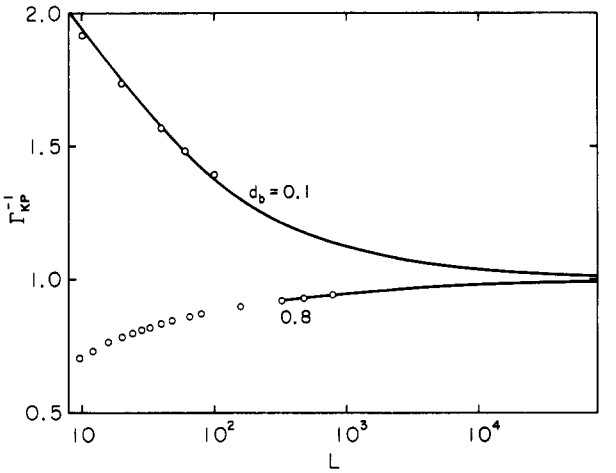


**Figure 1.** $\Gamma_{KP}^{-1}$ plotted against the logarithm of $L$ for the two cases of $d_b = 0.1$ and 0.8. The open circles represent the values for the KP touched-bead model, and the full curves represent those for the KP cylinder model with $d = 0.74d_b$.

Next, for the case of the HW touched-bead model, we construct an empirical interpolation formula for the factor $\Gamma$ defined by

$$[\eta]_{KR} = (\langle S^2\rangle/\langle S^2\rangle_{KP})^{3/2}[\eta]_{KR}^{(KP)}\,\Gamma(L,d_b;\kappa_0,\tau_0) \quad (27)$$

where $\langle S^2\rangle$ is the mean-square radius of gyration of the HW chain of total contour length $L$ and is given by eq 56 of ref 5 with $t = L$ and $\sigma = 0$. For later use, it is convenient to give the explicit expression for it,

$$\langle S^2\rangle = \frac{\tau_0^2}{\nu^2}\langle S^2\rangle_{KP} + \frac{\kappa_0^2}{\nu^2}\left[\frac{L}{3r}\cos\phi - \frac{1}{r^2}\cos(2\phi) + \frac{2}{r^3 L}\cos(3\phi) - \frac{2}{r^4L^2}\cos(4\phi) + \frac{2}{r^4L^2}e^{-2L}\cos(\nu L + 4\phi)\right] \quad (28)$$

where

$$\nu = (\kappa_0^2 + \tau_0^2)^{1/2} \quad (29)$$

$$r = (4 + \nu^2)^{1/2} \quad (30)$$

$$\phi = \cos^{-1}(2/r) \quad (31)$$

The factor $\Gamma$ thus defined has the following limiting values

$$\lim_{L\to 0}\Gamma = \lim_{L\to\infty}\Gamma = 1 \quad (32)$$

For the values of $\kappa_0$ and $\tau_0$ indicated by the filled points in the $(\kappa_0,\tau_0)$ plane of Figure 2 in the same ranges of $d_b$ and $N$ ($0.01 \le d_b \le 0.8$ and $2 \le N \le 1000$) as in the case of the KP touched-bead model above, we evaluate $\Gamma$ by the use of the values of $[\eta]_{KR}$ calculated from eq 16 with the numerical solution of eq 19 and the values of $[\eta]_{KR}^{(KP)}$ calculated from eq 22 with eq 23 and 25. The range of application of the interpolation formula for $[\eta]$ of the HW cylinder model previously obtained[3] is limited to the

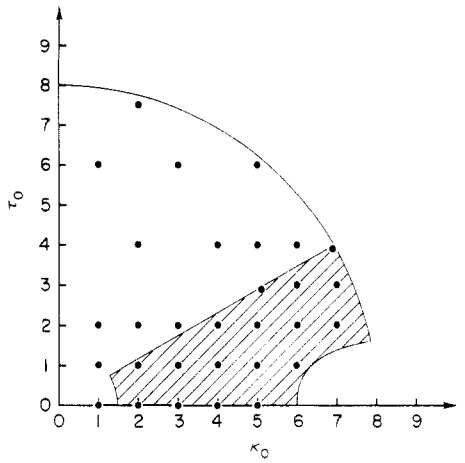


**Figure 2.** Values of $\kappa_0$ and $\tau_0$ plotted in a $(\kappa_0,\tau_0)$ plane. The filled circles represent the values of $\kappa_0$ and $\tau_0$ for which the factor $\Gamma$ is evaluated. Application of the interpolation formula for $[\eta]$ of the HW cylinder model presented previously[3] is limited to the shaded domain.

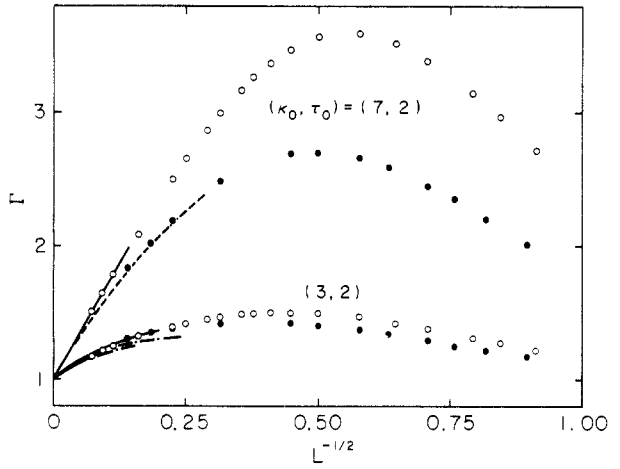


**Figure 3.** $\Gamma$ plotted against $L^{-1/2}$ for the two cases of $\kappa_0 = 7$ and $\tau_0 = 2$ and of $\kappa_0 = 3$ and $\tau_0 = 2$. The open and filled circles represent the values for the HW touched-bead model with $d_b = 0.2$ and 0.05, respectively, and the full curves represent the extrapolations. The broken curve represents the values for the HW cylinder model with $d = 0.74d_b$, and the chain curves represent those for the associated KP cylinder model with $d = 0.74d_b$.

shaded domain of Figure 2 and rather to the small values of $d$. Thus, except for such a limited range of its application, we cannot join $\Gamma$ for the HW touched-bead model to that for the HW cylinder model as we have done in the case of the KP chain.

In order to evaluate $\Gamma$ in the range of $N > 1000$ (or $L > 1000d_b$), we use the following maneuver. We make extrapolations to $\Gamma = 1$ at $L = \infty$ from the values of $\Gamma$ evaluated above in the range of $2d_b \leq L \leq 1000d_b$. In Figure 3 are shown the values of $\Gamma$ plotted against $L^{-1/2}$ for the two cases of $\kappa_0 = 7$ and $\tau_0 = 2$, (in the shaded domain of Figure 2) and of $\kappa_0 = 3$ and $\tau_0 = 2$ (outside the shaded domain), where the open and filled circles represent the calculated values for $d_b = 0.2$ and 0.05, respectively, and the full curves represent the extrapolations. The values for the HW cylinder model with the diameter $d$ properly chosen are available, for instance, in the case of $\kappa_0 = 7$, $\tau_0 = 2$, and $d_b = 0.05$, and in such a case, we may use those values, as represented by the broken curve in Figure 3. (Note that the relation $d = 0.74d_b$ may be retained for the HW chain as for the KP chain.) For the HW chain with $\kappa_0$ and $\tau_0$ outside the shaded domain, as in the case of $\kappa_0 = 3$ and $\tau_0 = 2$, the associated KP cylinder model

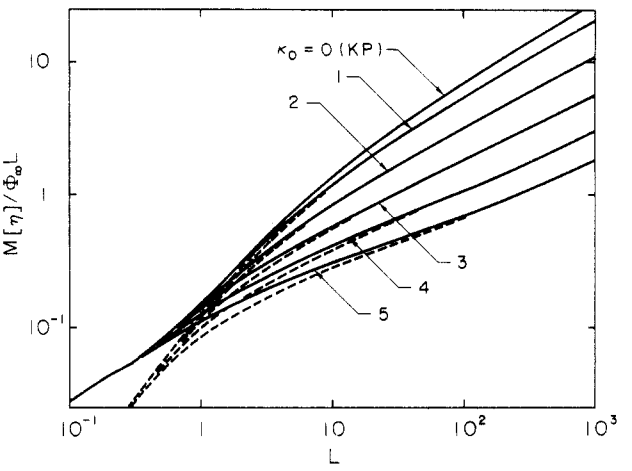


**Figure 4.** Double-logarithmic plots of $M[\eta]/\Phi_\infty L$ against $L$ for various values of $\kappa_0$ with $\tau_0 = 0$ and $d_b = 0.1$. The full and broken curves represent the values with and without the contribution of the Einstein spheres.

defined in ref 3 seems to give good approximate values in the range of large $L$, since the helical nature is not very strong. Those values calculated from eq 22 of ref 3 with $d = 0.74d_b$ are represented by the chain curves in Figure 3. Thus, we have made extrapolations (interpolations), as shown in the full curves in Figure 3.

A good approximation to $\Gamma$ thus evaluated has been found to be of the form

$$\Gamma = 1 + \kappa_0^2[e^{-\nu L/10}\sum_{i=1}^{2} A_i L^i + e^{-12/\nu L}\sum_{i=3}^{6} A_i L^{-(i-2)/2}] \quad (33)$$

with

$$A_i = \sum_{k,l=0}^{3}[\sum_{j=0}^{2} a_{ij}^{kl} d_b^{\,j} + \sum_{j=3}^{4} a_{ij}^{kl} d_b^{\,2(j-2)} \ln d_b]\nu^l \cos(k\pi\tau_0/\nu) \quad (34)$$

where $a_{ij}^{kl}$ are constants independent of $L$, $d_b$, $\kappa_0$, and $\tau_0$ and are given in Table II. The ranges of $\kappa_0$ and $\tau_0$ in which eq 27 with eq 28, 33, and 34 is applicable are such that $\kappa_0$ and $\tau_0$ satisfy the conditions, $\nu \leq 8$, $\kappa_0 \leq 7$, $\tau_0 \geq \kappa_0 - 5.5$, $\kappa_0 + \tau_0 > 0.5$, $\kappa_0 = 0.5i$, and $\tau_0 = j$ with $i$ the positive integer and $j$ the nonnegative integer; and the range of $d_b$ is limited to $0.01 \leq d_b \leq 0.8$ for $\tau_0 \geq 2\kappa_0$, to $0.01 \leq d_b \leq 0.6$ for $\tau_0 < 2\kappa_0$ and $\kappa_0 \leq 4$, to $0.01 \leq d_b \leq 0.4$ for $4 < \kappa_0 \leq 5$, and to $0.01 \leq d_b \leq 0.2$ for $\kappa_0 > 5$. In the above ranges of application of eq 27, the error in the value of $[\eta]$ calculated from eq 15 with eq 17 and 27 does not exceed 3% except for $\kappa_0 \geq 5$, in which domain the possible maximum error is 5%.

Finally, we examine the behavior of $[\eta]$ of the HW touched-bead model on the basis of the values calculated from eq 15 with eq 17 and 27. The dependence of $[\eta]$ on $L$ is similar to that of the HW cylinder model.[3] Thus,in this paper, we examine the dependence of $[\eta]$ on the helical nature and estimate the contribution $[\eta]_E$ to $[\eta]$ in the range of small $L$ (oligomer region). We consider only the special case of $\tau_0 = 0$ and $d_b = 0.1$ as a typical example. Note that the value 0.1 for $d_b$ corresponds to flexible chains. Figure 4 shows double-logarithmic plots of $M[\eta]/\Phi_\infty L$ against $L$ for this case. The full and broken curves represent the values with and without the contribution $[\eta]_E$, respectively, the numbers attached to the curves indicating the values of $\kappa_0$. Note that the helical nature becomes strong as $\kappa_0$ is increased. Some salient aspects of the behavior of $[\eta]$ are summarized as follows. First, in the limit of $L \to \infty$, the slope of the plot becomes equal to $^1/_2$, so that $[\eta]$ is proportional to $M^{1/2}$; i.e., the chain behaves as the unperturbed nondraining Gaussian

**Table II**
**Values of $a_{ij}^{kl}$ in Equation 34**

| $j$ | $k$ | $l$ | $a_{1j}^{kl}$ | $a_{2j}^{kl}$ | $a_{3j}^{kl}$ | $a_{4j}^{kl}$ | $a_{5j}^{kl}$ | $a_{6j}^{kl}$ |
|---|---|---|---|---|---|---|---|---|
| 0 | 0 | 0 | 4.3740 (−2)[a] | −5.7005 (−3) | 1.5783 | −6.1714 | 9.3510 | −2.1546 |
| 0 | 0 | 1 | −2.6683 (−2) | 5.0153 (−3) | −4.8764 (−1) | 2.2984 | −3.8827 | 9.4255 (−1) |
| 0 | 0 | 2 | 5.4865 (−3) | −9.9676 (−4) | 5.5772 (−2) | −3.0618 (−1) | 5.7135 (−1) | −1.5618 (−1) |
| 0 | 0 | 3 | −3.5146 (−4) | 5.6241 (−5) | −2.2400 (−3) | 1.4108 (−2) | −2.8824 (−2) | 9.0350 (−3) |
| 0 | 1 | 0 | −9.8759 (−3) | 9.3855 (−3) | 7.9863 (−2) | −1.6074 | 6.2428 | −5.5149 |
| 0 | 1 | 1 | 8.6995 (−3) | −8.0343 (−3) | 1.1442 (−1) | 4.2438 (−1) | −2.8537 | 2.6941 |
| 0 | 1 | 2 | −1.9806 (−3) | 2.0749 (−3) | −3.3841 (−2) | −1.5011 (−2) | 4.1581 (−1) | −4.2806 (−1) |
| 0 | 1 | 3 | 1.3292 (−4) | −1.6323 (−4) | 2.3114 (−3) | −1.3467 (−3) | −2.0080 (−2) | 2.2502 (−2) |
| 0 | 2 | 0 | 8.2175 (−3) | −1.3063 (−2) | −2.7468 (−1) | 7.5428 (−1) | −1.4470 | 1.7712 |
| 0 | 2 | 1 | −8.0286 (−3) | 1.1449 (−2) | 1.9329 (−1) | −6.2368 (−1) | 9.0207 (−1) | −8.7677 (−1) |
| 0 | 2 | 2 | 2.1003 (−3) | −2.8623 (−3) | −3.8882 (−2) | 1.4285 (−1) | −1.7885 (−1) | 1.4077 (−1) |
| 0 | 2 | 3 | −1.6036 (−4) | 2.0273 (−4) | 2.3772 (−3) | −9.6046 (−3) | 1.1084 (−2) | −7.2736 (−3) |
| 0 | 3 | 0 | −1.1933 (−2) | 8.4024 (−3) | −2.0610 (−1) | 1.9123 | −2.7095 | 9.5591 (−1) |
| 0 | 3 | 1 | 8.5897 (−3) | −7.8143 (−3) | 1.2410 (−1) | −1.0929 | 1.5158 | −5.0654 (−1) |
| 0 | 3 | 2 | −1.8595 (−3) | 2.0735 (−3) | −2.3313 (−2) | 2.0051 (−1) | −2.7595 (−1) | 8.8414 (−2) |
| 0 | 3 | 3 | 1.1845 (−4) | −1.6266 (−4) | 1.4186 (−3) | −1.1941 (−2) | 1.6443 (−2) | −5.0939 (−3) |
| 1 | 0 | 0 | 3.4750 (−1) | −8.3845 (−2) | 1.1307 | 3.5292 (1) | −8.9519 (1) | 5.8430 (1) |
| 1 | 0 | 1 | −2.3098 (−1) | 7.2274 (−2) | −2.9049 | −5.7669 | 3.3006 (1) | −2.9224 (1) |
| 1 | 0 | 2 | 5.9275 (−2) | −2.9808 (−2) | 7.2091 (−1) | 9.6138 (−2) | −5.1080 | 5.6318 |
| 1 | 0 | 3 | −4.7492 (−3) | 3.3823 (−3) | −4.1161 (−2) | −1.1742 (−2) | 3.1940 (−1) | −3.7437 (−1) |
| 1 | 1 | 0 | −9.9003 (−2) | −1.1472 (−2) | −1.6532 | 3.2134 (1) | −1.0126 (2) | 7.7624 (1) |
| 1 | 1 | 1 | 1.1904 (−1) | 2.6621 (−2) | 1.2605 (−1) | −1.4103 (1) | 5.2055 (1) | −4.3340 (1) |
| 1 | 1 | 2 | −3.0261 (−2) | −1.6424 (−2) | −2.7407 (−2) | 2.9139 | −1.0186 (1) | 8.7944 |
| 1 | 1 | 3 | 1.3699 (−3) | 2.4692 (−3) | 2.1815 (−2) | −2.6778 (−1) | 7.2290 (−1) | −6.0322 (−1) |
| 1 | 2 | 0 | −1.0729 (−1) | 3.9537 (−2) | 7.1921 (−1) | 1.1626 (1) | −3.8148 (1) | 2.8939 (1) |
| 1 | 2 | 1 | 1.0803 (−1) | −4.4421 (−2) | −6.3187 (−1) | −4.7301 | 2.0883 (1) | −1.8974 (1) |
| 1 | 2 | 2 | −3.1278 (−2) | 1.1258 (−2) | 9.4846 (−2) | 7.8525 (−1) | −4.0122 | 4.1390 |
| 1 | 2 | 3 | 2.7356 (−3) | −5.8429 (−4) | 7.6219 (−3) | −7.8339 (−2) | 2.7683 (−1) | −2.9243 (−1) |
| 1 | 3 | 0 | −1.1283 (−1) | 6.4364 (−3) | 7.5854 | −6.7640 (1) | 9.0024 (1) | −1.2847 (1) |
| 1 | 3 | 1 | 5.3218 (−2) | 3.8384 (−2) | −4.9448 | 4.2303 (1) | −5.5395 (1) | 7.5210 |
| 1 | 3 | 2 | −9.9555 (−3) | −1.9128 (−2) | 9.7517 (−1) | −8.1131 | 1.0367 (1) | −1.1041 |
| 1 | 3 | 3 | 1.1307 (−3) | 2.0767 (−3) | −5.9088 (−2) | 4.9207 (−1) | −6.2191 (−1) | 4.7344 (−2) |
| 2 | 0 | 0 | −8.7321 (−2) | −8.2387 (−1) | 5.2142 | −2.3419 (2) | 9.1804 (2) | −8.5028 (2) |
| 2 | 0 | 1 | −4.4202 (−1) | 8.7523 (−1) | 6.7368 | 2.2585 (1) | −3.1183 (2) | 3.4289 (2) |
| 2 | 0 | 2 | 3.0158 (−1) | −2.6845 (−1) | −2.7114 | 1.4998 (1) | 1.9266 (1) | −3.6278 (1) |
| 2 | 0 | 3 | −4.0674 (−2) | 2.9185 (−2) | 3.6072 (−1) | −2.3310 | 1.2420 | 6.5231 (−1) |
| 2 | 1 | 0 | 1.6450 | −8.3105 (−1) | 1.4327 (1) | −2.6724 (2) | 1.1038 (3) | −1.0509 (3) |
| 2 | 1 | 1 | −1.6847 | 8.2167 (−1) | 1.0634 (1) | 7.1381 | −3.8962 (2) | 4.5837 (2) |
| 2 | 1 | 2 | 5.6846 (−1) | −2.5421 (−1) | −6.7373 | 3.1702 (1) | 1.8997 (1) | −5.3356 (1) |
| 2 | 1 | 3 | −6.2738 (−2) | 2.9075 (−2) | 9.5012 (−1) | −4.7219 | 2.7531 | 1.1859 |
| 2 | 2 | 0 | −1.1464 | 8.2756 (−1) | 1.1256 (1) | −2.0060 (2) | 5.6208 (2) | −3.6057 (2) |
| 2 | 2 | 1 | 9.4501 (−1) | −07.3284 (−1) | 3.2532 | 7.0140 (1) | −2.5178 (2) | 1.5880 (2) |
| 2 | 2 | 2 | −2.4519 (−1) | 2.0333 (−1) | −3.8184 | 1.0338 | 2.6357 (1) | −1.6509 (1) |
| 2 | 2 | 3 | 1.9771 (−2) | −1.6959 (−2) | 6.0246 (−1) | −1.4806 | 1.5466 (−1) | 5.0002 (−2) |
| 2 | 3 | 0 | 7.5857 (−1) | 4.0032 (−1) | −2.9017 (1) | −6.6804 | 2.3024 (2) | −1.9069 (2) |
| 2 | 3 | 1 | −9.4206 (−1) | −3.6059 (−1) | 2.0700 (1) | −3.3473 (1) | −2.1948 (1) | 9.9298 |
| 2 | 3 | 2 | 2.6331 (−1) | 1.1902 (−1) | −4.0263 | 9.1264 | −9.9517 | 1.3157 (1) |
| 2 | 3 | 3 | −1.2637 (−2) | −1.2501 (−2) | 2.6890 (−1) | −6.4069 (−1) | 1.1255 | −1.4794 |
| 3 | 0 | 0 | 6.5184 (−1) | −6.2144 (−1) | 6.6916 | −3.2445 (1) | 2.1835 (2) | −2.4382 (2) |
| 3 | 0 | 1 | −7.6704 (−1) | 6.2903 (−1) | −4.0015 | −7.0646 | −4.9882 (1) | 6.9552 (1) |
| 3 | 0 | 2 | 2.8098 (−1) | −2.1177 (−1) | 4.2592 (−1) | 8.7627 | −8.4234 | 2.0351 |
| 3 | 0 | 3 | −3.0253 (−2) | 2.3329 (−2) | 7.9989 (−2) | −1.2561 | 1.7532 | −1.0013 |
| 3 | 1 | 0 | 4.8598 (−1) | −3.5124 (−1) | −1.4982 | −4.4677 | 1.8852 (2) | −2.5407 (2) |
| 3 | 1 | 1 | −4.9148 (−1) | 3.9521 (−1) | 7.8212 | −5.7644 (1) | −2.4845 | 7.4645 (1) |
| 3 | 1 | 2 | 2.0234 (−1) | −1.4935 (−1) | −3.8395 | 2.7669 (1) | −2.7516 (1) | 4.3975 |
| 3 | 1 | 3 | −2.8119 (−2) | 1.9441 (−2) | 5.5524 (−1) | −3.2869 | 3.8792 | −1.4953 |
| 3 | 2 | 0 | −6.5991 (−1) | 3.7925 (−1) | 4.8386 | −5.1154 (1) | 1.2690 (2) | −5.8648 (1) |
| 3 | 2 | 1 | 5.8571 (−1) | −3.5870 (−1) | 1.7015 | 1.0476 (1) | −3.7466 (1) | 2.2645 |
| 3 | 2 | 2 | −1.6411 (−1) | 9.9268 (−2) | −1.9989 | 4.8801 | −3.6094 | 7.6738 |
| 3 | 2 | 3 | 1.4356 (−2) | −7.6591 (−3) | 3.4061 (−1) | −1.0747 | 1.1634 | −1.0411 |
| 3 | 3 | 0 | 7.2831 (−2) | 2.8616 (−1) | −9.9441 (−2) | −1.1154 (2) | 2.0480 (2) | −4.5199 (1) |
| 3 | 3 | 1 | −2.6777 (−1) | −1.6349 (−1) | 4.5855 (−1) | 5.6364 (1) | −7.5629 (1) | −2.1635 (1) |
| 3 | 3 | 2 | 8.2542 (−2) | 3.2414 (−2) | −3.8354 (−2) | −9.9394 | 7.7662 | 1.1992 (1) |
| 3 | 3 | 3 | −1.2987 (−3) | −2.4754 (−3) | 1.4545 (−2) | 5.8013 (−1) | −2.3605 (−1) | −1.0952 |
| 4 | 0 | 0 | −5.0646 (−1) | −2.9893 | 1.5330 (1) | −9.6644 (2) | 4.1540 (3) | −4.1107 (3) |
| 4 | 0 | 1 | −1.6542 | 3.1431 | 2.5105 (1) | 1.4837 (2) | −1.6212 (3) | 1.8403 (3) |
| 4 | 0 | 2 | 1.2742 | −9.6873 (−1) | −1.0146 (1) | 4.5487 (1) | 1.5667 (2) | −2.4129 (2) |
| 4 | 0 | 3 | −1.6679 (−1) | 1.0564 (−1) | 1.3436 | −8.2377 | −3.2100 (−1) | 8.9303 |
| 4 | 1 | 0 | 4.7927 | −3.1651 | 7.3469 (1) | −1.2451 (3) | 4.9249 (3) | −4.7293 (3) |
| 4 | 1 | 1 | −5.0663 | 3.1295 | 3.0783 (1) | 1.4788 (2) | −1.9232 (3) | 2.2140 (3) |
| 4 | 1 | 2 | 1.8082 | −9.5242 (−1) | −2.3998 (1) | 1.0003 (2) | 1.5901 (2) | −3.0079 (2) |
| 4 | 1 | 3 | −2.1016 (−1) | 1.0774 (−1) | 3.4843 | −1.6826 (1) | 4.9561 | 1.1102 (1) |
| 4 | 2 | 0 | −2.1684 | 3.1140 | 5.0778 (1) | −8.1729 (2) | 2.3649 (3) | −1.5871 (3) |
| 4 | 2 | 1 | 1.5108 | −2.7877 | 8.5505 | 2.9690 (2) | −1.0986 (3) | 7.4775 (2) |
| 4 | 2 | 2 | −3.1496 (−1) | 7.7728 (−1) | −1.4006 (1) | −5.0408 (−1) | 1.2687 (2) | −9.3232 (1) |
| 4 | 2 | 3 | 1.8133 (−2) | −6.4934 (−2) | 2.2531 | −5.4765 | −9.3697 (−1) | 2.2453 |
| 4 | 3 | 0 | 2.9167 | 1.3875 | −9.4950 (1) | −3.0581 (2) | 1.5824 (3) | −1.2009 (3) |
| 4 | 3 | 1 | −4.0135 | −1.1704 | 7.1417 (1) | 2.1381 (1) | −4.7280 (2) | 3.0264 (2) |
| 4 | 3 | 2 | 1.2295 | 3.9572 (−1) | −1.4168 (1) | 9.2382 | 3.1019 (1) | 2.4680 |
| 4 | 3 | 3 | −7.7263 (−2) | −4.3431 (−2) | 9.6412 (−1) | −1.0662 | 4.5089 (−1) | −2.8997 |

[a] $a(n)$ means $a \times 10^n$.

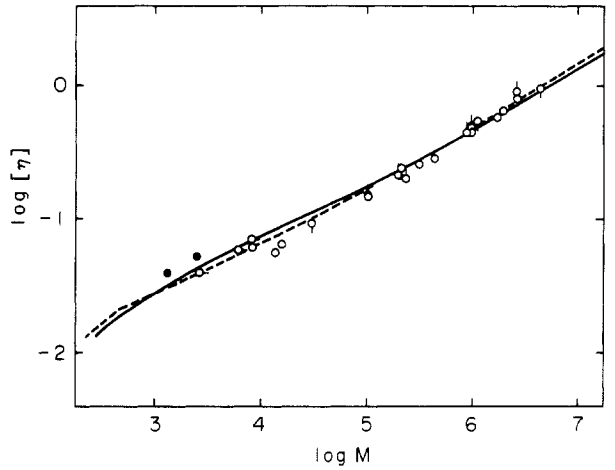


**Figure 5.** Analysis of the data for $[\eta]$ for atactic poly(methyl methacrylate) in various Θ solvents and benzene according to eq 35 with eq 36: (♀) in *n*-butyl chloride at 35 °C;[17] (○) in 4-heptanone at 31.5, 33.8, and 35.0 °C;[18] (♁) in acetonitrile at 45 °C;[18] (◇) in 3-heptanone at 33.7 °C and/or in methyl ethyl ketone–isopropyl alcohol (50% volume) at 25 °C;[19] (●) in benzene at 30 °C.[20] The full and broken curves represent the best-fit theoretical values as the HW and KP chains, respectively.

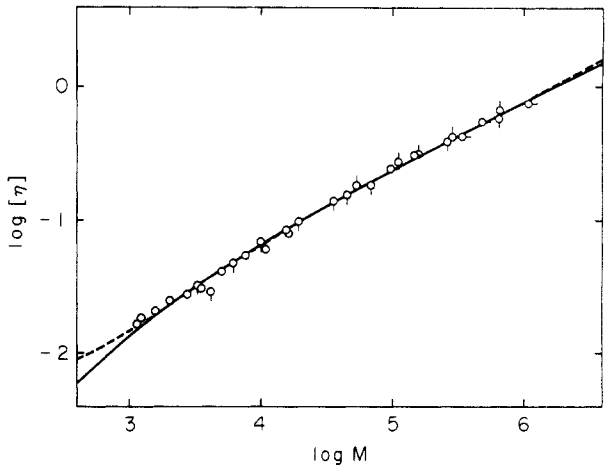


**Figure 6.** Analysis of the data for $[\eta]$ for poly(dimethylsiloxane) in various Θ solvents according to eq 35 with 36: (♁) in methyl ethyl ketone at 20 °C;[21] (◇) in bromocyclohexane at 28 °C;[22] (♀) in bromocyclohexane at 28 °C;[23] (○) in methyl ethyl ketone at 20 °C.[24] The full and broken curves represent the best-fit theoretical values as the HW and KP chains, respectively.

chain. Second, for the KP chain ($\kappa_0 = 0$), the slope of the plot first increases and then decreases to $^1/_2$ as $L$ is increased in the range of $L \geq 0.3$. It is important to see that the slope (for $\kappa_0 = 0$) is larger than $^1/_2$ in the range of $L$ displayed in Figure 3, as for typical stiff chains and perturbed nondraining Gaussian chains. Third, for the HW chain ($\kappa_0 \neq 0$), $[\eta]$ decreases with increasing $\kappa_0$ in the range of large $L$, and thus the slope of the plot becomes smaller than $^1/_2$. In contrast to the KP chain, for the chain of the strong helical nature, the slope of the plot first decreases and then increases to $^1/_2$ in the range of $L \geq 0.3$, as seen from the cases of $\kappa_0 = 4$ and 5. Fourth, from a comparison of the full curves with the broken curves, it is seen that the contribution $[\eta]_E$ is very important in the oligomer region.

## Analysis of Experimental Data

In this section, we make an analysis of experimental data for the intrinsic viscosity $[\eta]$ as a function of molecular weight $M$, taking as examples atactic poly(methyl methacrylate) (a-PMMA) and poly(dimethylsiloxane) (PDMS). In what follows, for convenience, we designate the reduced intrinsic viscosity by $[\bar{\eta}]$ to distinguish it from the unreduced $[\eta]$, and $[\bar{\eta}]$, $L$, $d_b$, $\kappa_0^{-1}$, and $\tau_0^{-1}$ are measured in units of $\lambda^{-1}$, all other quantities being unreduced unless specified otherwise.

As in the previous paper,[3] we consider double-logarithmic plots of $[\eta]$ (in dL/g) against $M$ by the use of the equation

$$\log [\eta] = \log (M[\bar{\eta}]/\Phi_\infty L) - \log (\lambda^2 M_L) - 2.542 \quad (35)$$

with

$$\log M = \log L + \log (M_L/\lambda) \quad (36)$$

where $M_L$ is the shift factor as defined as the molecular weight per unit (unreduced) contour length of the chain, $[\bar{\eta}]$ is given by eq 15 with eq 17 and 27 with $\Phi_\infty = 2.870 \times 10^{23}$, $\lambda^{-1}$ and $M_L$ being expressed in Å and Å$^{-1}$, respectively. Note that $M[\bar{\eta}]/\Phi_\infty L$ is a function of $L$, $d_b$, $\kappa_0$, and $\tau_0$. Thus the quantities $M_L/\lambda$ and $\lambda^2 M_L$ (and therefore $\lambda^{-1}$ and $M_L$) may be determined from a best fit of double-logarithmic plots of the theoretical $M[\bar{\eta}]/\Phi_\infty L$ (for proper $\kappa_0$, $\tau_0$, and $d_b$) against $L$ to those of the observed $[\eta]$ against $M$.

**Atactic Poly(methyl methacrylate).** Figure 5 shows double-logarithmic plots of $[\eta]$ against $M$. The open circles represent the experimental values for a-PMMA in various Θ solvents[17–19] and the filled circles, those for low molecular weights in benzene (good solvent) at 30 °C.[20] The full curve represents the best-fit theoretical values calculated as the HW chain from eq 15, 17, 27, and 35 with $\kappa_0 = 4.0$, $\tau_0 = 1.0$, $d_b = 0.19$, $\log (M_L/\lambda) = 3.16$, and $\log (\lambda^2 M_L) = -1.66$. From those, we obtain $\lambda^{-1} = 40.5$ Å, $M_L = 35.7$ Å$^{-1}$, and $d_b = 7.7$ Å ($d = 5.7$ Å). The broken curve represents the best-fit theoretical values calculated as the KP chain from eq 15, 17, 22, and 35 with $d_b = 0.8$, $\log (M_L/\lambda) = 2.44$, and $\log (\lambda^2 M_L) = -0.422$. We then obtain $\lambda^{-1} = 9.0$ Å, $M_L = 30.6$ Å$^{-1}$, and $d_b = 7.0$ Å ($d = 5.2$ Å). It is seen that the slope of the plot of the experimental data first decreases and then increases gradually with increasing $M$, and this behavior may be somewhat better explained by the HW chain than the KP chain. The value 9.0 Å for $\lambda^{-1}$ determined as the KP chain is unreasonably small.

**Poly(dimethylsiloxane).** Figure 6 shows double-logarithmic plots of $[\eta]$ against $M$ for PDMS in various Θ solvents.[21–24] In contrast to a-PMMA, the slope of the plot of the experimental data (open circles) decreases monotonically with increasing $M$, and it is difficult to determine the values of $\kappa_0$ and $\tau_0$ from a similar analysis of the data. Therefore, we assume that $\kappa_0$ and $\tau_0$ are the same as those determined from the analysis of the data for the mean-square dipole moment.[25] The full curve represents the best-fit theoretical values calculated as the HW chain with $d_b = 0.08$, $\log (M_L/\lambda) = 2.86$, and $\log (\lambda^2 M_L) = -1.47$, assuming $\kappa_0 = 2.5$ and $\tau_0 = 0$. From these, we obtain $\lambda^{-1} = 27.8$ Å, $M_L = 26.1$ Å$^{-1}$, and $d_b = 2.0$ Å ($d = 1.5$ Å). The broken curve represents the best-fit theoretical values calculated as the KP chain with $d_b = 0.32$, $\log (M_L/\lambda) = 2.7$, and $\log (\lambda^2 M_L) = -0.802$. We then obtain $\lambda^{-1} = 14.7$ Å, $M_L = 34.0$ Å$^{-1}$, and $d_b = 4.7$ Å ($d = 3.5$ Å). The value 34.0 Å$^{-1}$ for $M_L$ determined as the KP chain is too large compared to the value of 25.5 Å$^{-1}$ computed by taking the contour length as the length of the rotational isomeric state model chain fully extended to the all-trans conformation.

## Conclusions

We have evaluated the intrinsic viscosity of the helical wormlike touched-bead model taking into account the effect of the finite volume of the bead and have presented the interpolation formulas for it. They are valid even for

the large diameter of the bead and suffice for an analysis of experimental data for ordinary flexible chains. It has been shown that the effect of the finite volume cannot be ignored as far as the behavior of $[\eta]$ of flexible chains in the oligomer region is concerned. We have shown the two examples of flexible chains for which the behavior of $[\eta]$ may be better explained by the helical wormlike chain than by the ordinary wormlike chain or Gaussian chain, if the experimental data in the oligomer region are included.

In previous papers,[4,5] we evaluated various kinds of equilibrium properties on the basis of the HW model. From a comparison of these theoretical results with numerical results for the rotational isomeric state model or with experimental data, we showed that the HW chain can mimic the equilibrium conformational behavior of real polymer chains (both flexible and stiff) on the bond length or somewhat longer scales, and determined the HW model parameters of various polymers (see Table 1 of ref 4). The present analysis leads to the model parameters consistent with those previously determined, and we believe that $[\eta]$ is also a useful quantity for their determination. Therefore, a further experimental study of the behavior of $[\eta]$ of flexible chains over a wide range of the molecular weight including the oligomer region is required to clarify the local structure of flexible chains in solutions.

**Registry No.** Poly(methyl methacrylate), 9011-14-7.

## References and Notes


(1) Yamakawa, H.; Yoshizaki, T.; Fujii, M. *Macromolecules* **1977**, *10*, 934.
(2) Yamakawa, H.; Yoshizaki, T. *Macromolecules* **1979**, *12*, 32.
(3) Yamakawa, H.; Yoshizaki, T. *Macromolecules* **1980**, *13*, 633.
(4) Yamakawa, H. *Annu. Rev. Phys. Chem.* **1984**, *35*, 23.
(5) Yamakawa, H.; Fujii, M. *J. Chem. Phys.* **1976**, *64*, 5222 and following papers.
(6) Kratky, O.; Porod, G. *Recl. Trav. Chim. Pays-Bas* **1949**, *68*, 1106.
(7) Yamakawa, H.; Fujii, M. *Macromolecules* **1974**, *7*, 128.
(8) Kirkwood, J. G.; Riseman, J. *J. Chem. Phys.* **1948**, *16*, 565.
(9) Yoshizaki, T.; Yamakawa, H. *J. Chem. Phys.*, in press.
(10) Brenner, H. *Chem. Eng. Sci.* **1964**, *19*, 631.
(11) Yamakawa, H.; Yoshizaki, T. *J. Chem. Phys.* **1983**, *78*, 572.
(12) Zwanzig, R.; Kiefer, J.; Weiss, G. H. *Proc. Natl. Acad. Sci. U.S.A.* **1968**, *60*, 381.
(13) Perico, A.; Rossi, C. *J. Chem. Phys.* **1970**, *53*, 1217.
(14) Yamakawa, H.; Shimada, J.; Fujii, M. *J. Chem. Phys.* **1978**, *68*, 2140.
(15) Benoit, H.; Doty, P. *J. Phys. Chem.* **1953**, *57*, 958.
(16) Yamakawa, H. *Macromolecules* **1983**, *16*, 1928.
(17) Schulz, G. V.; Kirste, R. *Z. Phys. Chem. (Frankfurt Main)* **1961**, *30*, 171.
(18) Fox, T. G. *Polymer* **1962**, *3*, 111.
(19) Patrone, E.; Bianchi, U. *Makromol. Chem.* **1966**, *94*, 52.
(20) Fox, T. G.; Kinsinger, J. B.; Mason, H. F.; Schuele, E. M. *Polymer* **1962**, *3*, 71.
(21) Flory, P. J.; Mandelkern, L.; Kinsinger, J. B.; Shultz, W. B. *J. Am. Chem. Soc.* **1952**, *74*, 3364.
(22) Haug, A.; Meyerhoff, G. *Makromol. Chem.* **1962**, *53*, 91.
(23) Brzezinski, J.; Czlonkowska-Kohutnicka, Z.; Czarnecka, B.; Kornas-Calka, A. *Eur. Polym. J.* **1973**, *9*, 733.
(24) Dodgson, K.; Semlyen, J. A. *Polymer* **1977**, *18*, 1265.
(25) Yamakawa, H.; Shimada, J.; Nagasaka, K. *J. Chem. Phys.* **1979**, *71*, 3573.


# Thermotropic Polypeptides. 5. Temperature Dependence of Cholesteric Pitches Exhibiting a Cholesteric Sense Inversion


**Junji Watanabe* and Tatsuya Nagase**

*Department of Polymer Chemistry, Tokyo Institute of Technology, Ookayama, Meguro-ku, Tokyo 152, Japan.*

*Received June 22, 1987; Revised Manuscript Received August 6, 1987*


ABSTRACT: The cholesteric pitches were determined for the thermotropic cholesteric mesophases of poly[($\gamma$-benzyl L-glutamate)-*co*-($\gamma$-dodecyl L-glutamate)] with the dodecyl content of 58% in the wide temperature range from 100 to 250 °C. The pitches in an initial temperature range 100–130 °C are comparable to the wavelength of visible color and increase with rising temperature. After the pitches diverge at 195 °C, they decrease as temperature is raised further. In contrast to this anomalous behavior of pitches, the reciprocal pitches (measuring the twisting angles) vary smoothly with the temperature along a curve. The curve exhibits a remarkable variation of twisting angle at lower temperature and seems to approach a constant value at higher temperature, passing through zero at 195 °C. The latter indicates the cholesteric sense inversion. The results are discussed in terms of existing theories.


## Introduction

The cholesteric mesophase is generally regarded as a distorted form of the nematic mesophase and characterized by a macrohelical twist of pseudonematic layers. The existence of a finite pitch, thus, is a common feature of all cholesteric mesophases. The mutual twist of pseudonematic layers results from the microscopic structure of molecules and the nature of intermolecular interactions. According to the potential model based on the quadrapole–dipole interaction as well as the dipole–dipole one, Goossens[1] reached a conclusion that chirality is the major cause of the macroscopic twist. Unfortunately, Goossens also offered another conclusion that the pitch is insensitive to the temperature variation.

In actual situations, the pitch of cholesterics invariably depends on the temperature. Taking notice of this point, Keating[2] proposed the forces opposing the twist to be anharmonic in the chiral systems, so that a macroscopic twist results from the ensemble-averaging process. The theory predicts the pitch decreasing with the increasing temperature, which is in qualitative agreement with the experimental observation on most cholesterics.

There are, however, certain exceptional cases on the temperature variation of pitch. In one of them, the pitch increases with temperature. Also in another case, the pitch diverges, after which the helicity reverses and the pitch decreases as temperature is raised further. Such cases are hard to understand in terms of Keating's model.

The lyotropic cholesteric mesophases of polypeptides exhibit a temperature variation of pitch corresponding to the latter case as reviewed by Uematsu and Uematsu.[3] The typical example can be seen in the lyotropic systems of

0024-9297/88/2221-0171$01.50/0 